APPLICATION OF KALMAN FILTER TO ESTIMATE POSITION OF A MOBILE NODE IN INDOOR ENVIRONMENTS

A Thesis

Presented to

The Graduate Faculty of The University of Akron

In Partial Fulfillment

of the Requirements for the Degree

Master of Science

Mounika S. K. Gudipati

May, 2017

APPLICATION OF KALMAN FILTER TO ESTIMATE POSITION OF A MOBILE NODE IN INDOOR ENVIRONMENTS

Mounika S. K. Gudipati

Thesis

Approved:

Advisor
Dr. Shivakumar Sastry

Committee Member
Dr. Nghi Tran

Committee Member
Dr. Jin Kocsis

Accepted:

Interim Department Chair
Dr. Joan Carletta

Interim Dean of the College
Dr. Donald P. Visco, Jr.

Dean of the Graduate School
Dr. Chand K. Midha

Date

ABSTRACT

Estimating the position of mobile agents in indoor environments is a challenging problem especially when the estimates must be obtained using commercial, low cost devices. The work in this thesis presents experimental results that demonstrate the effectiveness of our approach, that integrates the signal strength data with sensed values of acceleration and angular velocity. A well-known framework called the Kalman Filter is used. To cope with the noise in the measured values, different versions of the Kalman Filter had to be used such as the Extended Kalman Filter and the Unscented Kalman Filter. This framework allowed us to systematically fuse the data from multiple sources to improve the accuracy of the position estimates. Our results demonstrate that positional accuracy of 0.8m within an 30m x 10m area is achieved. In the future, this work can be extended to further reduce the error in the location estimates by inclusion of encoders.

ACKNOWLEDGMENTS

First and foremost I would like to thank my advisor Dr.Shiva Sastry. He has taught me both consciously and unconsciously, how to approach an idea and to not fear to take a step towards it. I appreciate all his contribution of time, ideas and support in both technical and non-technical aspects, and inspirational discussions during my course of Master studies at the University of Akron.

My time at University of Akron was made enjoyable in a large part due to many friends. I would like to thank all my lab mates for their stimulating discussions and support for through the two years. A special thanks to my family for all their love and encouragement.

Finally, I sincerely acknowledge financial support from the University of Akron, US National Science Foundation (NSF) under the grant #IIS-1237069 to Dr. Sastry that financially supported my Graduate studies. Special thanks to Mr. John MacDonald in the Student Wellness and Recreation Center for providing the space to carry out the experiments.

TABLE OF CONTENTS

Page

LIST OF TABLES

LIST OF FIGURES

CHAPTER I

INTRODUCTION

Obtaining precise estimates of the position of a mobile node in indoor environments is an important problem in several emerging applications in areas such as Advanced Manufacturing, Internet of Things, and Healthcare Systems. The problem is especially challenging when the network connectivity must rely on commercially available, low-power wireless transceivers and the estimates must be precise. The received signal strength (RSS) is not reliable by itself to accurately estimate the position of the mobile node. Thus, it was necessary to augment the mobile node with additional inexpensive sensors to improve the accuracy of the estimates.

The problem of localization is very well studied in the literature [22, 49, 52, 27]. GPS based route navigation is a notable example in outdoor environments that is widely used all over the world. GPS based systems are not suitable in indoor environments because of poor signal reception and because the position estimates are only accurate to about two meters. As an example, in an asset management system for an advanced manufacturing or a healthcare facility, it is necessary to accurately know the position of objects that are about half a meter apart. The problem of estimating positions in indoor environments remains challenging especially when the applications demand precise estimates and the connectivity must rely on commercially

available transceivers.

The localization methods in the literature are based on measuring the distance between a mobile node and a fixed set of anchor nodes at known positions [17]. The distance between the nodes can be calculated using ToA (Time of Arrival), AoA (Angle of Arrival) or RSSI (Received Signal Strength Indicator) [27, 45]. While ToA and AoA can provide more accurate estimates, these approaches require additional, expensive, hardware. It is also not clear how much resolution these approaches can offer in indoor laboratory, healthcare and manufacturing environments.

Many of the low power transceivers record the value of RSS for every message they receive. Despite the easy access to the information, it is not feasible to use the RSS to estimate distance because of the irregularity of RF propagation [34] and because of the noise and nonlinearity in the RSS measurements. For this reason, we systematically explored how the precision could be improved by fusing the RSS data with data gathered from an inexpensive accelerometer and a gyroscope that was mounted on the mobile node. The results from our experiments demonstrate that the fusion improves the accuracy of the position estimates.

The Kalman Filter is a widely used recursive prediction-update based state estimator algorithm that can minimize error variance [44]. By viewing the position of the mobile node as its state, our aim was to minimize the error variance in these estimates. The prediction and update steps were combined via the Kalman gain that was calculated in each step to minimize the mean-square error. Such approaches are widely-reported in the literature in several areas including robot localization,

guidance and navigation and tracking [31, 18]. While many of the reports in the literature are based on simulation results, we found that the following reports were based on experiments in indoor environments [33, 10, 12]. The work in [33] used WiFi system and infrared sensors. The authors in [12] used accelerometer, gyroscope and compass and fused the data from these sensors. The report in [10] is closely related to our work; they used anchor nodes and an accelerometer. The anchor nodes were distributed evenly throughout the environment. In contrast, we designed the locations of the anchor nodes to minimize the errors in RSS estimates. Further, we dynamically assigned weights to the sensor values based on how close the values were to the estimated position.

The Kalman Filter is, however, known to provide an optimal estimate of the unknown state for a linear dynamic system with Gaussian distribution. The measurements required to assess the state of the mobile node, i.e., RSS, accelerations and the angular velocities were nonlinear. For this reason, we used an Extended Kalman Filter (EKF); the EKF used a first order linear approximation of the non-linearities. By integrating data from accelerometers and gyroscope mounted on the mobile node [9], we were able to reduce the error in position estimates. This reduction was, however, not good enough compared to what was reported in [33, 10] and, hence, we utilized an Unscented Kalman Filter (UKF); the UKF extracted key data points in the non-linear data and used these points to estimate the position. Experimental results demonstrate that this approach indeed provided precise position estimates.

The remainder of the thesis is organized as follows. Chapter 2 reviews the

background of various techniques for position estimation. Chapter 3 describes the problem and the system model designed is presented. The localization approach is mentioned in Chapter 4 and the experimental results that demonstrate the effectiveness of the approach used are discussed in Chapter 5. Finally, our conclusions and next steps are presented in Chapter 6.

CHAPTER II

BACKGROUND

Recent developments in low cost sensors and microcontrollers have enabled the deployment of ad-hoc wireless sensor networks for several applications [6, 1]. In many emerging scenarios in application areas such as healthcare and advanced manufacturing, it is necessary for the nodes to not only gather information but also to provide accurate estimates of position [36, 28]. These applications utilize position information to identify suitable services for the mobile node, or to assist the mobile nodes to maintain network connectivity.

Although GPS is widely used in outdoor localization [51], it is not suitable in large-scale indoor systems because of its cost, energy and poor connectivity [19]. Indoor localization is challenging because of multipath reflections, non-line of sight communications, presence of moving people that affect the indoor propagation of wireless channels, and the large number of obstacles that can attenuate the signals [25]. An extensive survey of indoor positioning techniques and solutions is presented in [48]. This survey describes several technologies such as radio frequency identifiers, cellular, inertial navigation units, ultra wide band communication systems and Bluetooth. The relative performance of such solutions were compared in terms of accuracy, precision, complexity, robustness and scalability.

Indoor localization techniques can be classified as ones that require the deployment of additional access points or beacons (infrastructure), ones that require exhaustive fingerprinting of the environment to characterize the distribution of signal strength, ones that are device-free, and ones that use measurement units. These approaches are described in the remainder of this section.

2.1 Infrastructure based Localization

Several indoor localization schemes using various infrared (IR), ultrasound, or radio-frequency (RF) devices have been reported in the literature [26]. The Active badge system is one example of early location aware application in which the person to be tracked carries a small tag which emits unique IR code every 15 seconds. A network of sensors that were placed in pre-determined locations gather the periodic IR waveforms and a central node processed the data to locate the individual using triangulation. Limited IR range and high maintenance costs were drawbacks of this system [43].

The infrastructure based localization systems can be classified as direction-based and distance-based systems. Direction based systems utilize antenna arrays and the angle of arrival (AoA) to infer the position of a mobile node; while these systems offer precise estimates, the cost and energy requirements are prohibitive [42]. Distance-based systems offer a cost-effective solution and rely on the RSS and the time of arrival (TOA). However, in indoor environments the propagation characteristics of wireless channels cause RSS to poorly relate to distance [23].

2.2 Localization using FingerPrinting

The fingerprinting based RSS approach is widely used [21]. There is a training phase and an online phase in this approach. A fingerprint database is created during the training phase; each fingerprint is a vector of RSS values from a set of anchor nodes. In the online phase, a mobile node measures the fingerprint vector of RSS from the same set of anchor nodes estimates its position using a distance measure or by estimating the likelihood [16, 7]. The most challenging aspects of fingerprinting based method is to formulate the distance calculation that can measure similarity between observed RSS and known RSS fingerprints. The drawback of this approach is that it is expensive to build a fingerprint database in the training phase and the database needs to be re-established when the application scenario changes [50].

2.3 Device-Free Localization

Device-free techniques utilize the installed wireless data networks to detect changes in the environment and track the location of entities without attaching any special devices to the entities [47]. It is useful in many applications such as intrusion detection and tracking for homes and offices, and security systems such as motion detection and video surveillance [38, 53]. Computer vision based approaches are considered as device-free; however, these techniques depend on ambient light and can only track objects that are within the line of sight of the camera. Radio tomography based

techniques [46] can track moving objects; however, these approaches are not scalable because of their high cost.

2.4 Localization using Inertial Sensors

Sensor-based position estimation is interesting because consumer mobile devices such as smartphones are being equipped with sensors such as magnetometer, accelerometer, gyroscopes and barometer [3]. These sensors measure the direction, acceleration, rotational velocity and altitude, respectively. They do not depend on the environment where the entities are located. However, the sensed values are not fully reliable because of sensor drift and integration errors [14]. Inertial sensors are used in mobile robots to improve odometry, flight stabilization or autonomous hovering of helicopters and quadrotors [15]. In human tracking, miniature inertial sensors are integrated into clothes or shoes. In [39], the authors propose a method to localize a resident in an indoor environment by using distributed binary sensors and body activity information obtain from IMU. Additionally, the combination of inertial sensors with wireless signal sensors allows for correction of errors accumulated during integration of inertial sensor data. However due to their size, weight and power consumption, commercially available IMU's are not suited for certain applications like miniature aerial vehicles [30].

Dead reckoning is a method of deducing current position based on past known position and current displacement and altitude. The authors in [40], propose an approach of tracking technique using walking patterns where a pedestrian dead reckon-

ing (PDR) is used to accurately detect and track steps. SmartPDR is another proposal using inertial sensors that shows a position estimate error of about 1.6m [20]. Other approaches combine PDR with other techniques such as Wifi, radio signal fingerprinting [5].

2.5 Sensor Fusion based Localization

Sensor fusion techniques can improve the accuracy of the estimates by integrating data from multiple sources. Kalman filter based data fusion methods have been widely studied. A combination of inertial sensors and cameras for self-localization is introduced in [29]. In [32], an IMU, wheel encoders and GPS were integrated using a Kalman Filter (KF) to obtain an outdoor 3-D localization solution. The authors in [8], consider the problem of locating moving target receiver by using unsynchronized stationary beacons. A bank of Kalman filters is used to fuse estimated positions and velocities of targets with the received symbols and timestamps. The authors in [11] fused gyroscope and magnetometer measurements using a Fuzzy rule base and a Kalman Filter.

This thesis presents a localization solution using the Extended Kalman Filter (EKF) and an Unscented Kalman Filter to fuse RSS data with acceleration and angular velocities that are measured on the mobile node. We use weighting scheme in which the most reliable data is used to accurately estimate the position of the mobile node.

CHAPTER III

SYSTEM MODEL

This chapter describes the system model, the development platform, the measurement inputs, their calibration, and how Kalman gain was computed.

3.1 System Description

The system comprises a single mobile node and a set of anchor nodes. Each node had an integrated wireless transceiver; the mobile node broadcast reference messages to the anchor nodes and the anchor nodes that are within the range of transmission respond to these reference messages. RSS values were recorded both on the mobile node and the anchor nodes. The mobile node was equipped with an accelerometer and gyroscope to measure the acceleration and angular velocity of the mobile node.

The IRIS mote was used as the experimental platform. This mote has an 8-bit ATMega1281 microcontroller that is optimized for low power operations and can be programmed using standard C language. The mote is integrated with an AT86RF230, IEEE 802.15.4 compliant, transceiver operating in 2.45GHz ISM band. The microcontroller and the transceiver exchange information via the SPI protocol. This mote was used both as the anchor nodes and as the mobile node.

3.2 System Model

The state of the mobile node was modeled in terms of its position, velocity and acceleration in a two-dimensional space as

$$\mathbf{X}_k = [x_0, y_0, v_x, v_y, a_x, a_y, \theta_x, \theta_y],^T$$

where (x, y) is the position, v_x and v_y are the velocities along the x and y axes, a_x and a_y are the accelerations, and θ_x and θ_y are the corresponding angular velocities. The state of the system, evolves in discrete steps, k. In each step, the Kalman filter approach predicts the state of the system, $\mathbf{X}_k^{(-)}$, and corrects this prediction using measurements to obtain the corrected state, $\mathbf{X}_k^{(+)}$. The approach relies on the state transition model, $\mathbf{A}$, to predict the next state as

$$\mathbf{X}_k^{(-)} = \mathbf{A}(\mathbf{X}_{k-1}^{(+)}) + \mathbf{w}_k, \tag{3.1}$$

where $\mathbf{w}_k \sim N(0, \mathbf{Q})$ is a random variable that represented the noise with zero mean and covariance matrix $\mathbf{Q}$, and

$$\mathbf{A} = \begin{bmatrix} 1 & 0 & dt & 0 & dt^2/2 & 0 \\ 0 & 1 & 0 & dt & 0 & dt^2/2 \\ 0 & 0 & 1 & 0 & dt & 0 \\ 0 & 0 & 0 & 1 & 0 & dt \\ 0 & 0 & 0 & 0 & 1 & 0 \\ 0 & 0 & 0 & 0 & 0 & 1 \end{bmatrix}. \tag{3.2}$$

Here, dt represents the time interval for each step and

$$\mathbf{Q} = q \begin{bmatrix} dt^4/4 & 0 & dt^3/2 & 0 & dt^2/2 & 0 \\ 0 & dt^4/4 & 0 & dt^3/2 & 0 & dt^2/2 \\ dt^3/2 & 0 & dt^2 & 0 & dt & 0 \\ 0 & dt^3/2 & 0 & dt^2 & 0 & dt \\ dt^2/2 & 0 & dt & 0 & 1 & 0 \\ 0 & dt^2/2 & 0 & dt & 0 & 1 \end{bmatrix}, \tag{3.3}$$

where q is a tuning parameter that must be obtained through experiments; this covariance matrix captures the effect of factors such as friction or sudden impulses that are not accounted for in the model for the mobile node.

3.3 Calibration

Since the measurements are a critical aspect for this approach, all sensors measurements, including RSS measurements, must be calibrated. The purpose of calibration is to choose suitable parameters that account for the performance of the actual devices employed and the specific indoor environment in which the devices operate.

The acceleration data were gathered using the LIS344AL accelerometer. The signal from this device, $\mathbf{acc}_t$, was assumed to account for acceleration ($\mathbf{a}_t$), gravity ($\mathbf{g}_t$), small sensor bias ($\mathbf{b}_{a,t}$), and measurement noise ($\mathbf{v}_{a,t}$)

$$\mathbf{acc}_t = \mathbf{a}_t - \mathbf{g}_t - \mathbf{b}_{a,t} + \mathbf{v}_{a,t}, \tag{3.4}$$

where $\mathbf{v}_{a,t} \sim N(0, \sigma^2)$.

To calibrate the acceleration measurements, samples were collected when the mobile node was stationary and the average values of accelerations along the x and y axes were computed. These averages represent the effect of gravity and other measurement errors that could arise because of temperature sensitivity, improper mounting of the accelerometer, or other unknown issues. During the operation of the mobile node, these average values were subtracted from the measured accelerations, i.e., a_x and a_y.

Similarly, the angular velocity measurements were also calibrated. The LSM6DS3 gyroscope was used and the signal from this device, $\mathbf{y}_{g,t}$, was assumed to comprise the angular velocities (θ_t), a gyroscope bias $\mathbf{b}_{g,t}$, and white measurement noise ($\mathbf{v}_{g,t}$),

i.e.,

$$\mathbf{y}_{g,t} = \theta_t - \mathbf{b}_{g,t} + \mathbf{v}_{g,t}, \tag{3.5}$$

where $\mathbf{v}_{g,t}$ is white noise process with covariance $\mathbf{Q}_{g,t}$

$$\mathbf{v}_{g,t} \sim N(0, \sigma^2_{g,t}) \tag{3.6}$$

The gyroscope was calibrated by collecting data when the mobile node was stationary and averaging the samples to account for bias errors, similar to the accelerometer.

The RSS is particularly sensitive to the environment in which the nodes operate. In free space, the Friis equation relates the power of the received signal, the power of the transmitted signal, the wavelength, distance, and the antenna gains of the transmitter and the receiver [4]. In a typical indoor environment, several factors cause attenuation of the transmitted signal as the distance increases. For this reason, we consider a simpler path loss model called the log normal propagation model [37] that characterizes the indoor channel for 802.11 wireless local area networks at 2.4GHz which is applicable for our system consisting of IRIS mote [35].

$$M_i = -(10\ \mathcal{C}_i \log_{10} \mathcal{D}_i - \mathcal{S}_i), \tag{3.7}$$

where RSS is the average received power in dB at a distance of $\mathcal{D}$ m; $\mathcal{C}$ is a propagation constant that is characteristic of the environment, and $\mathcal{S}$ is the received power in dB

at a distance of 1 m.

To calibrate RSS measurements, we first computed $\mathcal{S}$ and $\mathcal{C}$ for the environment. Recall, our system uses a set of anchor nodes, $\{\mathcal{A}_1, \mathcal{A}_2, \cdots, \mathcal{A}_N\}$. Our measurements revealed that the RSS values were different with respect to each anchor node and hence we computed $\mathcal{S}_i$ and $\mathcal{C}_i$ with respect to each anchor node, $1 \leq i \leq N$. The average value of RSS_i measured at the mobile node for $\mathcal{A}_i$ was determined by placing the mobile node at 1m from each anchor node.

The propagation constant $\mathcal{C}_i$ accounts for the environment in which the mobile node must operate. For this reason, we collected RSS samples by moving the mobile node over a 10 m distance in steps of 0.5 m. For each, distance step, s, in this range, we collected 100 RSS samples from each anchor node and computed the average $RSS_{s,i}$ with respect to the anchor node $\mathcal{A}_i$ at step s. Let $\mathcal{D}_{s,i}$ represent the distance between the mobile node and the anchor node $\mathcal{A}_i$ at step s. Then,

$$\mathcal{C}_i = -\frac{1}{60} \sum_{s=1}^{60} \frac{M_{s,i} - \mathcal{S}_i}{10 \log_{10} \mathcal{D}_{s,i}}. \tag{3.8}$$

Finally, we computed the average received power at the mobile node, $M_{s,i}$, with respect to anchor node $\mathcal{A}_i$, as

$$M_{s,i} = RSS_{s,i} - 91,$$

as specified in the RF230 datasheet [2].

3.4 Measurement Model

The Kalman filter approach relies on measurements to reduce the error in the position estimates. This is accomplished in two steps - first, the estimated measurements, $\hat{\mathbf{Z}}_k$, are predicted using the predicted state of the system

$$\hat{\mathbf{Z}}_k = h(\mathbf{X}_k^{(-)}) + \mathbf{v}_k \tag{3.9}$$

where $\mathbf{v}_k \sim N(0, \mathbf{R})$ and $h(.)$ is an observation function that relates the state at time step k to the measurement.

We assumed that the measurement errors in the different sensors were independent and, hence, set $\mathbf{R}$ to be a diagonal matrix. Based on our choice of sensors, we used $\mathbf{R}_1$ to account for the covariance between RSS measurements, and $\mathbf{R}_2$ to account for the covariance between the data gathered from the inertial sensors, i.e., accelerometer and gyroscope.

$$\mathbf{R}_1 = \left[diag(\sigma_{M_1}^2, \sigma_{M_2}^2, \cdots, \sigma_{M_N}^2) \right] \tag{3.10}$$

$$\mathbf{R}_2 = \left[diag(\sigma_{a_x}^2, \sigma_{a_y}^2, \sigma_{\dot{\theta}_x}^2, \sigma_{\dot{\theta}_y}^2) \right] \tag{3.11}$$

The values of $\mathbf{R}$ are obtained as described in Section 4. These values characterize the errors in the measurement because of various inaccuracies.

An observation function was designed using the model in Equation (3.7).

Ideally, such an observation function would be

$$h(\mathbf{X}_k^{(-)}) = -\begin{bmatrix} S_1 - 10\ \mathcal{C}_1 \log_{10}(d_1) \\ S_2 - 10\ \mathcal{C}_2 \log_{10}(d_2) \\ \cdots \\ S_N - 10\ \mathcal{C}_N \log_{10}(d_N) \end{bmatrix}, \tag{3.12}$$

where d_i is the current distance between the mobile node and anchor node $\mathcal{A}_i$ in step k.

The Kalman filter framework requires both the state dynamics and the measurement characteristics to be linear and the noise distribution to be Gaussian [44]. When a non-linear function is applied to a Gaussian random variable, the resulting random variable is no longer Gaussian and, hence, the Kalman filter requirement is not satisfied [13]. Since the RSS measurements were not linear, we used an Extended Kalman Filter (EKF) framework to estimate the positions. EKF provides a differentiable function that approximates the non-linearities introduced by the RSS measurements by locally linearizing at current time step around the estimated mean. A Jacobian matrix $\mathbf{H}_k$ represents the partial derivative of the observation function [24]. Thus, a Jacobian is useful to define how the elements of the observation function affect the state of the system,

$$\mathbf{H}_k = -\begin{bmatrix} \frac{\partial h^{(i)}}{\partial x_0} & \frac{\partial h^{(i)}}{\partial y_0} \end{bmatrix}. \tag{3.13}$$

To get accurate position estimates, we are only interested in how the current observation of the position, (x_0, y_0), affects the state.

The choice of sensors in our system, constrains us to two actual measurements. The first measurement, $\mathbf{Z}_k^1$, captures the received power at the mobile node with respect to each anchor node, $\mathcal{A}_i$,

$$\mathbf{Z}_k^1 = \Big[M_1, M_2, \cdots, M_N \Big],^T$$

where M_i is the average received power at the mobile node from $\mathcal{A}_i$.

The second measurement, $\mathbf{Z}_k^2$, captures the accelerations and angular velocities,

$$\mathbf{Z}_k^2 = \Big[a_x, a_y, \theta_x, \theta_y \Big].^T$$

The actual measurements above and the estimated measurements shown in Equation (3.9) are combined to correct the predicted state of the system through the Kalman gain.

3.5 Kalman Gain Computation

The Kalman Gain, $\mathbf{K}_k$, is an adaptive parameter in the Kalman filtering algorithm that indicates how much weightage must be assigned to the actual measurement ($\mathbf{Z}_k$) vs. the estimated measurement ($\hat{\mathbf{Z}}_k$) in step k.

The difference between the measurements is used to obtain the corrected state as

$$\mathbf{X}_k^{(+)} = \mathbf{X}_k^{(-)} + \mathbf{K}_k[\mathbf{Z}_k - \hat{\mathbf{Z}}_k]. \tag{3.14}$$

In each step, the Kalman gain is itself updated as

$$\mathbf{K}_k = \mathbf{P}_k^{(-)}\mathbf{H}_k^T[\mathbf{H}_k\mathbf{P}_k^{(-)}\mathbf{H}_k^T + \mathbf{R}]^{-1}, \tag{3.15}$$

where $\mathbf{P}_k^{(-)}$ is the predicted error covariance that is computed as

$$\mathbf{P}_k^{(-)} = \mathbf{A}\mathbf{P}_{k-1}^{(+)}\mathbf{A}^T + \mathbf{Q}. \tag{3.16}$$

Kalman gain for the next step, $k+1$, is selected to minimize the updated error covariance,

$$\mathbf{P}_k^{(+)} = [\mathbf{I} - \mathbf{K_k}\mathbf{H_k}]\mathbf{P}_\mathbf{k}^{(-)}. \tag{3.17}$$

3.6 Unscented Kalman Filter

The Unscented Kalman Filter (UKF) is a derivative free alternative to the EKF that provides a more accurate estimate of the state in the presence of state or measurement nonlinearities [41]. This is because, the EKF uses only first order terms of the Taylor expansion of the non- linear system, which introduces errors in estimating the posterior distribution of the state [13]. Unlike the EKF, the UKF does not approximate the non-linear process and observation models, it uses true non- linear models and

approximates the distribution of the state. In the UKF the state is still represented by the Gaussian random variable, but is specified by using a set of chosen sample points. These sample points capture the mean and covariance of the random variable, and when propagated through the non- linear system, capture posterior mean and covariance.

The Unscented transform is the basic idea behind the UKF which provides a method to calculate the mean and covariance of the random variable which undergoes non-linear transformation. In this section we describe all the steps that are needed to perform an estimation update using UKF. Initially, when $k = 0$, the state $\mathbf{X}_k$ and the error covariance $\mathbf{P}_k$ are set to some known values. The data from the sensors, i.e., RSS, a_x, a_y and θ_x, θ_y, must be prefiltered by adapting the value of q in Equation (3.3). Decreasing q will cause the filter to rely more on the predicted state and less on actual measurements, and vice versa.

The prediction step of the UKF is similar to one used above for the EKF as shown in Equation 3.1. The UKF relies on sigma points in its correction step. Sigma samples are a set of sample points,$\{W^i, \mathcal{X}^i\}$, that are selected to represent the state distribution from the preceding step. One can select 2n+1 weighted sigma samples where, n represents the dimensionality of state representation.

$$\mathcal{X}_k^0 = \mathbf{X}_k^{(-)} \tag{3.18}$$

$$\mathcal{X}_k^i = \mathbf{X}_k^{(-)} + \sqrt{(n+\lambda)\mathbf{P}_k^{(-)}} \quad \forall\ i = 1 \cdots n \tag{3.19}$$

$$\mathcal{X}_k^i = \mathbf{X}_k^{(-)} - \sqrt{(n+\lambda)\mathbf{P}_k^{(-)}} \quad \forall\ i = n+1 \cdots 2n \tag{3.20}$$

where, λ, is a scaling parameter that determines the spread of the sigma points around the mean. It is expressed as

$$\lambda = \alpha^2(n+\kappa) - n,$$

where, κ and α are unscented parameters that are used to influence how far the sigma points are away from the mean. Typical values for α is 10^{-3} and $\kappa \geq 0$.

The next step after computing the sigma points is to assign a weight to each sigma point. Weights are chosen such that

$$\sum_{i=0}^{2n} W_m^{(i)} = \sum_{i=0}^{2n} W_c^{(i)} = 1 \tag{3.21}$$

where

$$W_m^{(i)} = \begin{cases} \frac{n}{n+\lambda}, & if\ i = 0 \\ \frac{1}{2(n+\lambda)}, & \forall i = 1...2n \end{cases} \tag{3.22}$$

$$W_c^{(i)} = \begin{cases} W_m^{(0)} + (1 - \alpha^2 + \beta), & if\ i = 0 \\ \frac{1}{2(n+\lambda)}, & \forall i = 1...2n \end{cases} \tag{3.23}$$

α, β and λ are unscented parameters with $\beta = 2$ and the other two parameters as defined above; $W_m^{(i)}$ represents the weights assigned to the mean estimate and $W_c^{(i)}$ represents the weights assigned to the covariance estimates.

The sigma points computed are projected through the observation function $h(.)$

$$\gamma_k^i = h(\mathcal{X}_k^i) \qquad \forall i = 1.....2n \tag{3.24}$$

The weighted sigma points are recombined to produce the predicted measurement and predicted measurement covariance

$$\hat{Z}_k = \sum_{i=0}^{2n} W_m^{(i)} \gamma_k^i \tag{3.25}$$

$$\mathbf{P}_{Z_K Z_k} = \sum_{i=0}^{2n} W_c^{(i)} [\gamma_k^i - \hat{Z}_k][\gamma_k^i - \hat{Z}_k]^T \tag{3.26}$$

The state- measurement covariance matrix is given by

$$\mathbf{P}_{X_k Z_k} = \sum_{i=0}^{2n} W_c^{(i)} [\mathcal{X}^i - \mathbf{X}_k^{(-)}][\gamma^i - \hat{\mathbf{Z}}_k]^T \tag{3.27}$$

The UKF Kalman Gain is given by

$$\mathbf{K}_k = \mathbf{P}_{X_k Z_k} \mathbf{P}_{Z_K Z_k}^{-1} \tag{3.28}$$

As with the Kalman Filter, updated state is the predicted state plus innovation weighted kalman gain

$$\mathbf{X}_k^{(+)} = \mathbf{X}_k^{(-)} + \mathbf{K}_k[\mathbf{Z}_k - \hat{\mathbf{Z}}_k]. \tag{3.29}$$

And the updated covariance is the predicted covariance, minus the predicted measurement covariance, weighted by Kalman Gain.

$$\mathbf{P}_k^{(+)} = [\mathbf{P}_k^{(-)} - \mathbf{K}_k \mathbf{P}_{X_k Z_k} \mathbf{K}_k^T]. \tag{3.30}$$

CHAPTER IV

LOCALIZATION APPROACH

This chapter presents an overview on the the localization approach. First, the method for obtaining the position estimates using the inertial sensors and RSS is discussed. Finally, fusion of the data using Kalman Filters as a basis is described.

4.1 Position Estimation using inertial sensors

The inertial system is composed of an accelerometer and a gyroscope, measuring accelerations (a_x and a_y) and angular velocities (θ_x and θ_y) respectively along x and y axes. As discussed in the section 3, acceleration due to gravity is subtracted from the acceleration signal and the remaining acceleration is integrated once, over the duration when the mobile node is moving, to obtain the velocity, and again to obtain the position. The orientation of the mobile node is tracked by integrating the angular velocity signals. However, the errors in the accelerometer and gyroscope signals and those introduced by numerical integration propagate to the position and orientation estimates of the mobile node. Kalman filter is thus used to model these errors and obtain a better estimate.

4.2 Position Estimation using RSS

To estimate the unknown position of mobile node, at least three anchor nodes must be able to detect and measure mobile node's signal strength. The mobile node stores its position coordinates and value of average received power from each of the anchor nodes, $\{\mathcal{A}_1, \mathcal{A}_2, \cdots, \mathcal{A}_N\}$. The distance between mobile node and each anchor node is calculated from the average received power M_i as

$$\mathcal{D}_i = 10^{\frac{S_i - M_i}{10\mathcal{C}_i}}. \tag{4.1}$$

We use Trilateration to estimate the position of the mobile node (x_0, y_0) based on estimated distances $\mathcal{D}_i$ between mobile node and of at least three anchor nodes with positions(x_{A_i}, y_{A_i}).

The actual distance between the mobile node and each of the anchor node is given by

$$r_i = \sqrt{(x_0 - x_{A_i})^2 + (y_0 - y_{A_i})^2} \tag{4.2}$$

The error e_i, between the estimated distance, d_i, and the actual distance, r_i is given by

$$e_i = d_i - \sqrt{(x_0 - x_{A_i})^2 + (y_0 - y_{A_i})^2}. \tag{4.3}$$

Ideally we would like to minimize this error

$$e_i = d_i - \sqrt{(x_0 - x_{A_i})^2 + (y_0 - y_{A_i})^2} = 0. \tag{4.4}$$

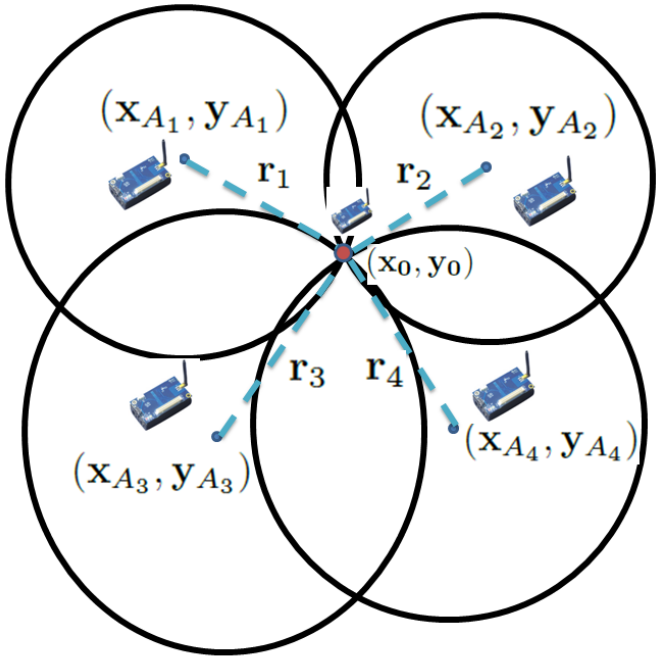

Figure 4.1: Intuitively, the trilateration approach involves drawing circles with the anchor nodes as the centers; for each anchor node, the distance estimated using average received power is the radius of the circle. The mobile node lies at the intersection of these circles.

Solving for 4.2, we get

$$\begin{aligned} 2x_0(x_{A_N} - x_{A_i}) + 2y_0(y_{A_N} - y_{A_i}) = r_i^2 - r_N^2 \\ -x_{A_i}^2 - y_{A_i}^2 + x_{A_N}^2 + y_{A_N}^2. \end{aligned} \tag{4.5}$$

This equation is linear and can be represented as

$$Fm = U$$

where

$$F = \begin{bmatrix} 2(x_{A_N} - x_{A_1}) & 2(y_{A_N} - y_{A_1}) \\ 2(x_{A_N} - x_{A_2}) & 2(y_{A_N} - y_{A_2}) \\ \vdots & \\ 2(x_{A_N} - x_{A_{N-1}}) & 2(y_{A_N} - y_{A_{N-1}}) \end{bmatrix} \tag{4.6}$$

$$U = \begin{bmatrix} r_1^2 - r_N^2 - x_{A_1}^2 - y_{A_1}^2 + x_{A_N}^2 + y_{A_N}^2 \\ r_2^2 - r_N^2 - x_{A_2}^2 - y_{A_2}^2 + x_{A_N}^2 + y_{A_N}^2 \\ \vdots \\ r_{N-1}^2 - r_N^2 - x_{A_{N-1}}^2 - y_{A_{N-1}}^2 + x_{A_N}^2 + y_{A_N}^2 \end{bmatrix} \tag{4.7}$$

and

$$m = \begin{bmatrix} x_0 \\ y_0 \end{bmatrix}$$

The least squares solution for $Fm = U$, is given by

$$m = (F^T F)^{-1} F^T U$$

Hence, the estimated position of the mobile node can be computed from above equation.

4.3 Fusing the Position Estimates

The approach to measurement fusion used in our model is to weight the individual measurements from each sensor and then track those fused measurements by a

Kalman Filter to obtain an estimate of the state vector. Since the measurement noise is independent for accelerometer sensor and RSS, the equation for fusing the measurement vectors ${Z_k}^1$ and ${Z_k}^2$, for minimum square estimate is given by

$$\mathbf{Z}_k = \mathbf{Z}_k^1 + \mathbf{R}_1(\mathbf{R}_1 + \mathbf{R}_2)^{-1}(\mathbf{Z}_k^2 - \mathbf{Z}_k^1), \tag{4.8}$$

where $\mathbf{R}_1$ and $\mathbf{R}_2$ are the covariance matrices of the measurement vector of sensor 1 and sensor 2. The measurement noise covariance matrix of fused measurement $\mathbf{Z}_k$ is derived by

$$\mathbf{R} = [(\mathbf{R}_1)^{-1} + (\mathbf{R}_2)^{-1}]^{-1}. \tag{4.9}$$

The fused estimate measurements are then used to estimate the state vector $\mathbf{X}_k$ by applying Extended Kalman Filter and Unscented Kalman Filter equations.

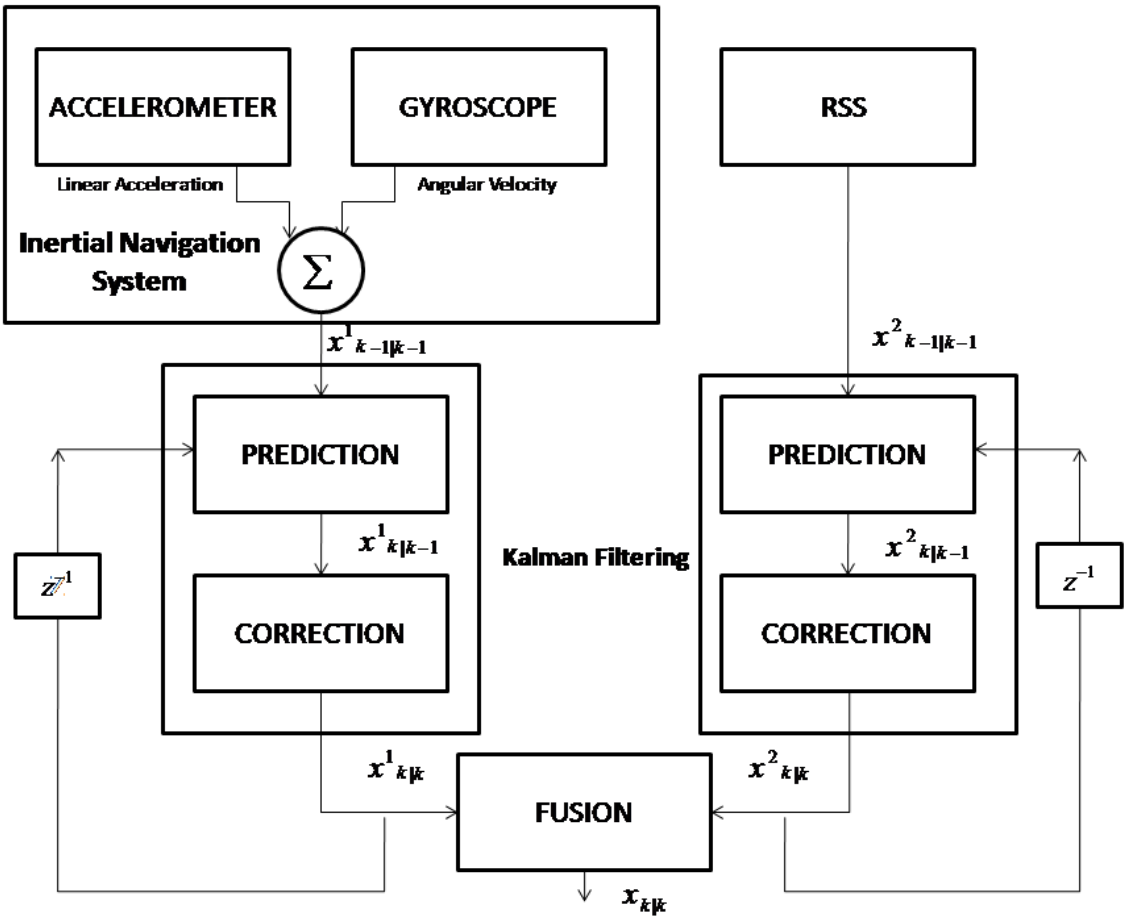

Figure 4.2: Acceleration and RSS data are fused to estimate the position of the mobile node.

CHAPTER V

RESULTS

This chapter presents experimental results to demonstrate the effectiveness of the approach described in the preceding chapters.

5.1 Experimental Setup

All the results were obtained through experiments conducted in a large indoor area of 10m x 30m. Human activity in the room was minimal and other than the materials that were used for construction, no other furniture or laboratory equipment were in the space. Two sets of experiments were conducted to understand the effect of increasing the number of anchor nodes on the accuracy of position estimates. In the first set of experiments, four anchor nodes were placed in the four corners of the experimental area; in the second set, two more anchor nodes were added. All the anchor nodes were placed after carefully measuring the signal strength of the RF communications.

Table 5.1 presents the error between the actual distance between the mobile node and the anchor node and the distance computed using RSS. Notice that the error trend has a low positive slope when the distance between the mobile node and the anchor node is less than five meters. When the communication distance is larger

than 5m, the error increased. This is likely because of the degradation of the wireless signal due to obstacles, reflections, multipath effects, or other such factors. These data helped to determine how to locate the anchor nodes.

Table 5.1: Range error of different environmental parameters calculated by two nodes by comparing the real distance and experimental distance that is extracted from RSS-model.

Parameters	1M	2M	3M	4M	5M	6M	7M	8M	9M
n = 1.03	1.45	1.68	2	2.58	3.02	5.86	6.21	7.01	7.98
n = 3.1	1.62	1.97	2.12	2.45	2.98	5.38	6.43	7.22	8.01
n = 1.72	1.54	1.68	1.93	2.12	2.71	5.41	5.89	6.97	6.98
n = 1.2	1.38	1.75	2.04	2.23	2.61	5.29	5.73	6.89	7.17
Average	1.49	1.77	2.02	2.35	2.83	5.49	6.07	7.02	7.77

The orientation of the antennas of the anchor nodes also affects the signal strength. In the experiments conducted, the antennas for all the nodes were oriented at 90 degrees relative to the mounting surface. The average RSS values and the sensor data and the position estimates collected in the mobile node were sent over wireless links to a base station.

5.2 Calibration

It is critical to calibrate the environment before relying on the RSS measurements for estimating distance. The following steps were carried out to calibrate the motes:

1. The mobile node was rotated through six positions in steps of 60 degrees to understand the effects of antenna orientation.

2. In each orientation of the mobile node, 100 beacon messages were sent and all the anchor nodes responded to each beacon message by returning the RSS value and Link Quality Indicator (LQI) value for each beacon message. These data were collected by the mobile nodes and the average RSS and LQI values were computed over the 100 messages. The Packet Error Rate was computed by the mobile node as the ratio of the number of ACK messages received to the number of beacon messages, i.e., 100, that were sent.

As described in Chapter: 3, the values for signal propagation constant, $\mathcal{C}$, and reference transmitting power, $\mathcal{S}$, were determined. The resulting model parameters are shown in Table 5.2. These data reveal that the average received power does not vary linearly with distance and, in fact, the signal propagation constant is different for each anchor node.

Table 5.2: The IDs of the anchor nodes are shown in the first column; for each anchor node, the transmitted power (in dBm) at a distance of 1m and the path loss constant obtained from calibration are shown.

Node ID	$\mathcal{S}$	$\mathcal{C}$
12	-31.79	1.84
13	-43.64	3.1
14	-40.42	1.72
15	-30.9	1.2
16	-42.4	1.34
17	-34.55	1.5

Comparison between the average received power computed Vs. calibrated received power for anchor node $\mathcal{A}_{12}$ and $\mathcal{A}_{16}$ as the distance changed is shown in Figure 5.1. While RSS decreases with increasing distance, there are other variations

that are likely caused because of the effects of fading and reflections. Thus, small changes in the position of the mobile node may result in a significant difference in the received power.

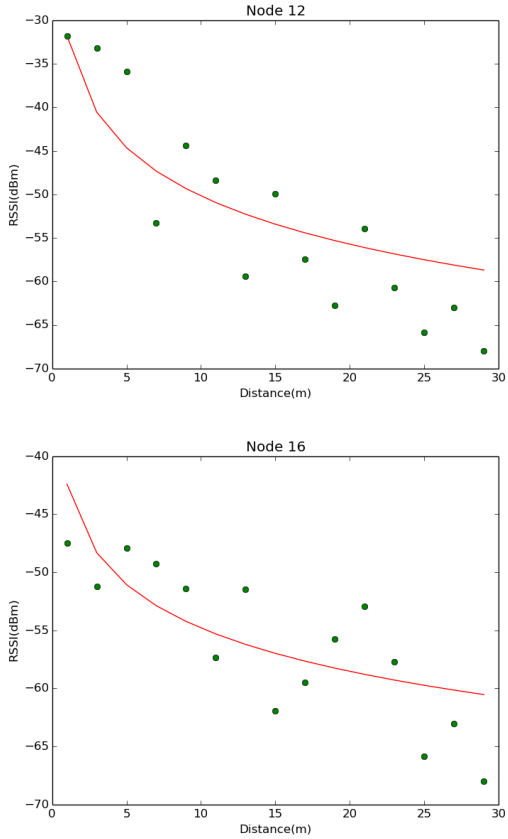

Figure 5.1: The measured RSS values confirmed that there is a non-linear relationship with distance. The relative location of the nodes significantly affect the measured value.

5.3 Mobile Node Localization

The mobile and anchor nodes were programmed to exchange data packets; from each message RSS, LQI values were extracted. When the mobile node received a message,

it also gathered acceleration and angular velocity from its sensors. The mobile node was moved along a linear path and a U-path over the length of the room. The average, maximum and minimum values were computed at each position of the mobile node. The acceleration and orientation values which were fused and sent to the base station at every 1m distance. Accuracy was determined by comparing the position estimated by this system with the predicted position of the mobile node.

Figure 5.2 shows the distance traveled by the mobile node as obtained from the results of the accelerometer. The graph represents the acceleration along x-axis where position and velocity estimates along x-axis are obtained by double and single integration of the acceleration values respectively. Vibrations were minimized by performing the experiment on a smooth surface. The position estimation with information from accelerometer is susceptible to errors because of integration errors.

Integration errors are a major challenge. Because of drift that accumulates over time, and uncertainties in bias factors, the position cannot be estimated accurately over longer periods of time. Similarly, small errors in orientation can yield large error in position estimate. For these reasons, it was observed that overall performance could be improved by combining the accelerometer data with data from a gyroscope.

Figure 5.3 shows the angular velocity of the mobile node as obtained from the results of the gyroscope. The orientation information obtained from gyroscope helps to account for directionality of motion. The error in gyroscope is due to constant bias error.

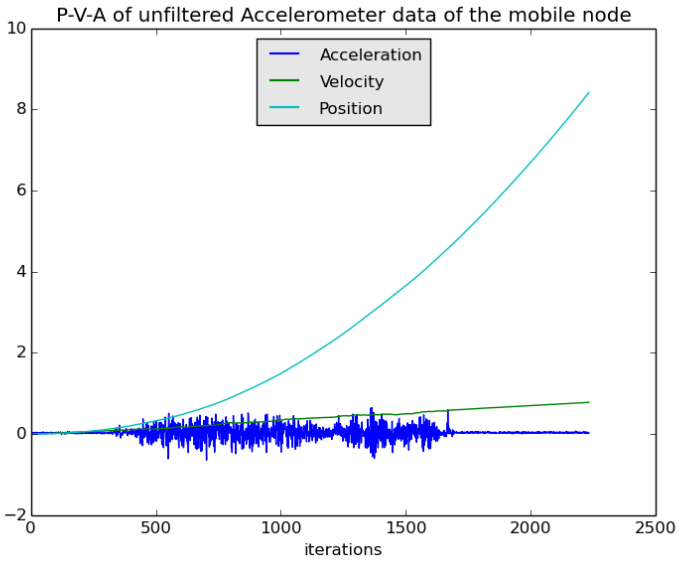

Figure 5.2: The noise in the accelerometer data is a likely contributor to the error in the computed velocity and position.

After calculating the estimated distances, they were compared with the actual distances to evaluate the performance. Figure 5.4 presents the actual path of the mobile node (solid line) and the position estimates obtained using methods described in the preceding chapters. The top left figure shows the position estimates obtained by using just the RSS values. The top right figure shows estimates obtained by fusing the RSS values with acceleration and angular velocity data using a a linear Kalman Filter. The bottom left figure shows the estimates obtained when an EKF was used to fuse the RSS, acceleration and angular velocity data. The bottom right figure shows the improvement obtained using the UKF. Observe that the error between the actual path and the estimated positions is least when using the UKF.

Figure 5.5 presents the actual path of the mobile node and the estimated

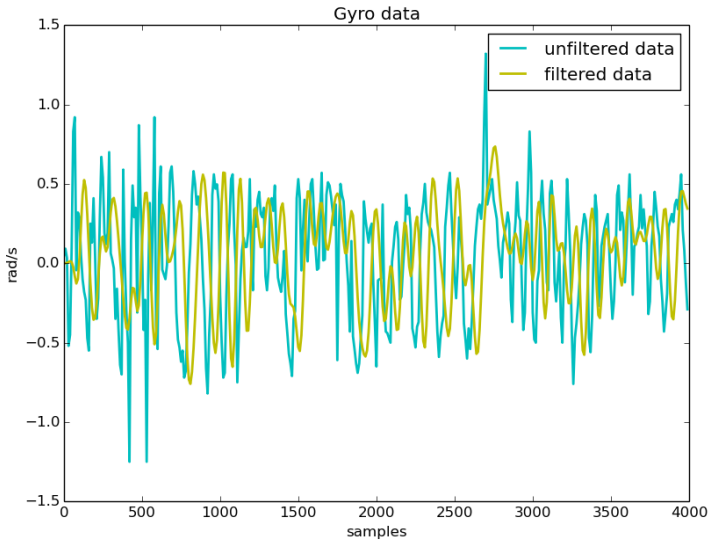

Figure 5.3: Inclusion of gyroscope helps to compensate drift and calibration error in accelerometer

positions when using six anchor nodes. Notice that the variation from the actual path of the mobile node is further reduced when compared with the results shown in Figure 5.4.

Figure 5.6 presents the average localization error in the different scenarios - without fusion, fusion using Kalman Fileter, Extended Kalman Filter and Unscented Kalman Filter. Observe that the inertial sensors cannot provide acceptable localization accuracy by themselves. Additional functionality and sensor fusion techniques using EKF and UKF could be used to improve the accuracy.

To understand the effect of turns on the accuracy of position estimates, further experiments were conducted by moving the mobile node along a U-path. Figure 5.7 shows the trajectory of the mobile node and the accuracy obtained using the

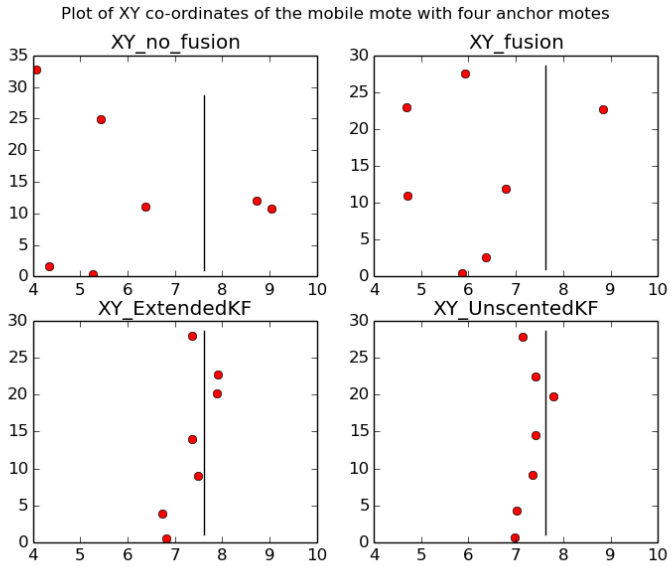

Figure 5.4: Fusing the data from the accelerometer and gyroscope with the RSS data helps to reduce the variation in the position estimate with respect to the actual position, which implies that the accuracy is improved compared with individual sensor position estimation.

different methods for fusing data described above. Notice, the error is high at the turns. This is likely because of the change in antenna orientation and the lack of a more precise model to capture the dynamics of the mobile node.

The results in this chapter demonstrate that it is important to fuse data from multiple sensors to obtain accurate position estimates. The RSS values are affected by the environment conditions, distance and the orientation of antennas. The EKF and the UKF provided more accurate estimates when compared with the estimates obtained using a linear Kalman Filter.

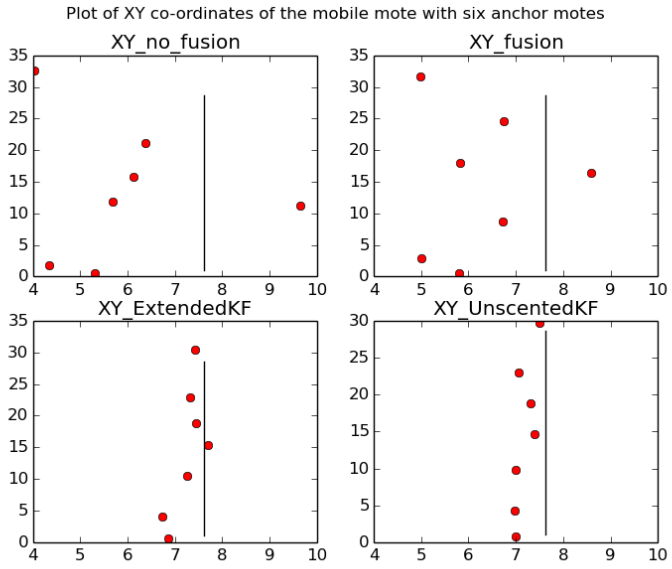

Figure 5.5: Fusing RSS data with acceleration and angular velocity data using the Unscented Kalman Filter provides the most accurate position estimates even when using six anchor nodes.

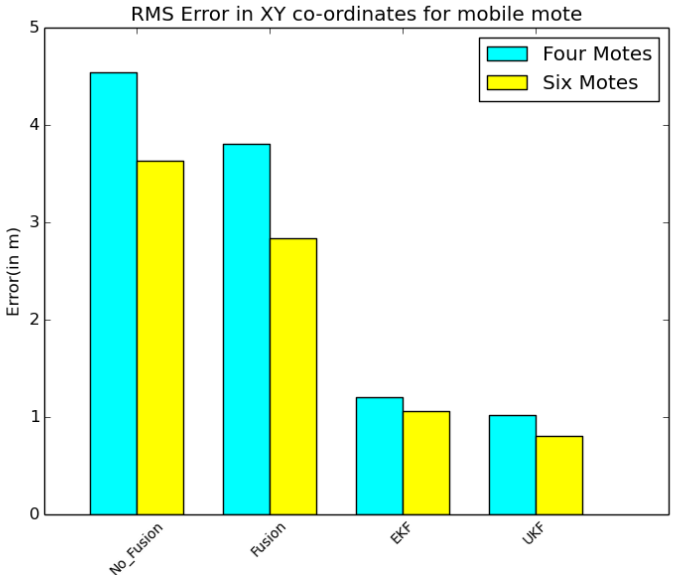

Figure 5.6: Localization accuracy evaluation in a linear path

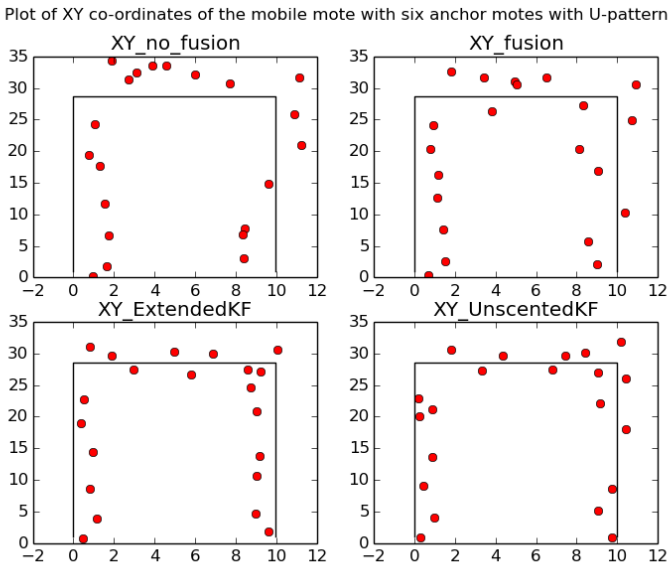

Figure 5.7: There is significant error while starting or stopping a turn when compared to error in linear motion

CHAPTER VI

CONCLUSION

The thesis presented an approach to estimate the position of a mobile node in an indoor environment that used an Extended Kalman Filter and an Unscented Kalman Filter. The position estimate was obtained using RSS values collected by exchanging beacon messages with anchor nodes. These data were fused with data obtained from an accelerometer and a gyroscope on the mobile node. We compared the accuracy of the position estimate that was obtained without fusing data from the two sources and by fusing the data based on experimental results. The results showed that fusing the estimates obtained using RSS and inertial sensors(accelerometer and gyrscope) data reduced the absolute position error from 3.83m to 0.8m in case of a linear path and 4.9m to 1.01m in case of U-path. Thus, we can conclude that fusing data from multiple sources is indeed a viable strategy to improve the position estimates.

The results showed that a large number of parameters must be manipulated to achieve accurate position estimates. In particular, the orientation of the nodes, the transmission power used, calibration and other environmental effects affect the fidelity of the estimates. If the transmission power is too high, the differences in RSS values are not significant. Several experiments were conducted to derive the values of S and $\mathcal{C}$ and these values can be different for each anchor node.

In the future, this approach can be extended to a more comprehensive set of experiments including encoders. In addition, it would be useful to understand how the accuracy of such an approach compares with what can be achieved using the GPS system in emerging outdoor applications.

BIBLIOGRAPHY

[1] A. Alhalafi, L. Sboui, R. Naous, and B. Shihada. gTBS: A green task-based sensing for energy efficient wireless sensor networks. *IEEE Conference on Computer Communications Workshops*, 2016.

[2] ATMEL. *AVR Low Power 2.4 GHz Transceiver for Zigbee IEEE 802.15.4, 6-LoWPAN, RF 4CE, and ISM Applications*, 2009.

[3] E. R. Bachmann, X. Yun, and R. B. McGhee. Sourceless tracking of human posture using small Inertial/Magnetic sensors. *Proceedings of the IEEE International Symposium on Computational Intelligence in Robotics and Automation*, 2:822–829, 2003.

[4] C. A. Balanis. *Antenna Theory: Analysis and Design*. Wiley-Interscience, 2005.

[5] R. Ban, K. Kaji, K. Hiroi, and N. Kawaguchi. Indoor positioning method integrating pedestrian dead reckoning with magnetic field and WiFi fingerprints. *Eighth International Conference on Mobile Computing and Ubiquitous Networking*, pages 167–172, 2015.

[6] M. K. D. Barma and S. Das. Data gathering mechanism of mobile data collector in Wireless Sensor Network. *International Conference on Internet of Things and Applications*, pages 401 – 405, 2016.

[7] C. Beder and M. Klepal. Fingerprinting based localisation revisited: A rigorous approach for comparing RSSI measurements coping with missed access points and differing antenna attenuations. *International Conference on Indoor Positioning and Indoor Navigation*, 2012.

[8] J. Bordoy, A. Traub-Ens, A. Sadr, J. Wendeberg, F. Hoflinger, C. Schindelhauer, and L. Reindl. Bank of Kalman filters in closed-loop for robust localization using unsynchronized beacons. *IEEE Sensors Journal*, 16:7142–7149, 2016.

[9] J. Borenstein, H. R. Everett, L. Feng, and D. Wehe. Mobile robot positioning: sensors and techniques. *Robotic Systems*, 14:231–249, 1997.

[10] W. Chai, C. Chen, E. Edwan, J. Zhang, and O. Loffeld. INS/WiFi based indoor navigation using Adaptive Kalman Filtering and vehicle constraints. *Positioning Navigation and Communication*, 2012.

[11] H. Chung, C. Hou, and Y. Chen. Indoor intelligent mobile robot localization using fuzzy compensation and Kalman filter to fuse the data of Gyroscope and Magnetometer. *IEEE Transactions on Industrial Electronics*, pages 6436–6447, 2015.

[12] A. Colombo, D. Fontanelli, D. Macii, and L. Palopoli. Flexible indoor localization and tracking based on a wearable platform and sensor data fusion. *IEEE Transactions on Instrumentation and Measurement*, 2014.

[13] F. Daum. Nonlinear filters: beyond the Kalman Filter. *IEEE Aerospace and Electronic Systems Magazine*, 20:57 – 69, 2005.

[14] J. Georgy, A. Noureldin, M. J. Korenberg, and M. M. Bayoumi. Modeling the stochastic drift of a MEMS-based Gyroscope in Gyro/Odometer/GPS integrated navigation. *IEEE Transactions on Intelligent Transportation Systems*, 11:856 – 872, 2010.

[15] I. Gumusboga and E. Kiyak. An integrated navigation system design for quadrotors. *Sensor Data Fusion: Trends, Solutions, Applications*, pages 1 – 5, 2015.

[16] Z. Guowei, X. Zhan, and L. Dan. Research and improvement on indoor localization based on RSSI fingerprint database and K-nearest neighbor points. *International Conference on Communications, Circuits and Systems*, pages 68 – 71, 2013.

[17] G. Han, J. Jiang, C. Zhang, T. Q. Duong, M. Guizani, and G. K. Karagiannidis. A survey on mobile anchor node assisted localization in wireless sensor networks. *IEEE Communication Surveys and Tutorials*, 18:2220–2243, 2016.

[18] Y. Huang, S. Zhang, and Y. Jing. An indoor mobile localization strategy based on Particle Filter in NLOS environment. *Control and Decision Conference*, pages 6518 – 6522, 2016.

[19] J. H. Kang, K. J. Park, and H. Kim. Analysis of localization for drone-fleet. *International Conference on Information and Communication Technology Convergence*, pages 533 – 538, 2015.

[20] W. Kang and Y. Han. SmartPDR: Smartphone-based pedestrian dead reckoning for indoor localization. *IEEE Sensors Journal*, pages 2906–2916, 2015.

[21] M. B. Kjaergaard. A taxonomy for radio location fingerprinting. *Proceedings of the Third International Symposium on Location and Context Awareness*, pages 139–156, 2007.

[22] K. Laith and J. Peter. Scaled Unscented Kalman Filter for RSSI-based indoor positioning and tracking. *Next Generation Mobile Applications, Services and Technologies*, pages 132 – 137, 2015.

[23] K. C. Lee, A. Oka, E. Pollakis, and L. Lampe. A comparison between Unscented Kalman Filtering and Particle Filtering for RSSI-based tracking. *7th Workshop on Positioning Navigation and Communication*, pages 157 – 163, 2010.

[24] T. Lefebvre, H. Bruyninckx, and J. D. Schutter. Location systems for ubiquitous computing. *IEEE Transactions on Automatic Control*, 2001.

[25] F. Lemic, V. Handziski, A. Wolisz, T. Constambeys, C. Laoudias, S. Adler, S. Schmitt, and Y. Yang. Experimental evaluation of RF-based indoor localization algorithms under RF interference. *International Conference on Localization and GNSS*, pages 1 – 8, 2015.

[26] H. Liu, H. Darabi, P. Banerjee, and J. Liu. Survey of wireless indoor positioning techniques and systems. *Systems, Man and Cybernetics Part C: Applications and Reviews IEEE Transactions*, 37:1067–1080, 2007.

[27] X. Y. Liu, S. Aeron, V. Aggarwal, X. Wang, and M. Y. Wu. Adaptive sampling of RF fingerprints for fine-grained indoor localization. *IEEE Transactions On Mobile Computing*, 15:2411–2423, 2016.

[28] G. B. Moon, S. Chun, M. B. Hur, and G. I. Jee. A robust indoor positioning system using two-stage EKF SLAM for first responders in an emergency environment. *International Conference on Control, Automation and Systems*, pages 707–711, 2013.

[29] N. Mostofi, M. Elhabiby, and N. El-Sheimy. Indoor localization and mapping using camera and inertial measurement unit (IMU). *Position, Location and Navigation Symposium*, pages 1329–1335, 2014.

[30] J. Muller, A. Rottmann, L. M. Reindl, and W. Burgard. A probabilistic sonar sensor model for robust localization of a small-size blimp in indoor environments using a Particle filter. *IEEE International Conference on Robotics and Automation*, 2009.

[31] T. T. V. Nguyen, M. D. Phung, T. H. Tran, and Q. V. Tran. Mobile robot localization using fuzzy neural network based Extended Kalman Filter. *International Conference on Control System, Computing and Engineering*, pages 416 – 421, 2012.

[32] E. North, J. Georgy, M. Tarbouchi, U. Iqbal, and A. Noureldin. Enhanced mobile robot outdoor localization using INS/GPS integration. *International Conference on Computer Engineering and Systems*, pages 127–132, 2009.

[33] A. S. Paul and E. A. Wan. RSSI-based indoor localization and tracking using Sigma-Point Kalman Smoothers. *IEEE Selected Topics in Signal processing*, 2009.

[34] R. M. Pellegrini, S. Persia, D. Volponi, and G. Marcone. RF propagation analysis for Zigbee sensor network using RSSI measurements. *International Conference on Wireless Communication, Vehicular Technology, Information Theory and Aerospace and Electronic Systems Technology*, 2011.

[35] R.Akl, D.Tummala, and X.Li. Indoor propagation modeling at 2.4 GHz for IEEE 802.11 networks. *International Multi-Conference on Wireless and Optical Communications: Conference on Communication Systems and Applications, Optical Communication Systems and Networks, Wireless Networks and Emerging Technologies, Wireless SENSOR Networks*, 2006.

[36] A. Redondi, M. Tagliasacchi, M. Cesana, L. Borsani, P. Tarro, and F. Salice. LAURA Localization and ubiquitous monitoring of patients for health care support. *IEEE 21st International Symposium on Personal, Indoor and Mobile Radio Communications Workshops*, pages 218–222, 2010.

[37] T. K. Sarkar, J. Zhong, K. Kyungjung, A. Medouri, and M. Salazar-Palma. A survey of various propagation models for mobile communication. *IEEE Antennas and Propagation Magazine*, 45:51 – 82, 2003.

[38] S. Savazzi, S. Sigg, M. Nicoli, V. Rampa, S. Kianoush, and U. Spagnolini. Device-free radio vision for assisted living: Leveraging wireless channel quality information for human sensing. *IEEE Signal Processing Magazine*, 33:45 – 58, 2016.

[39] T. Sztyler and H. Stuckenschmidt. On-body localization of wearable devices: An investigation of position-aware activity recognition. *IEEE International Conference on Pervasive Computing and Communications*, pages 1 – 9, 2016.

[40] A. Vidal, J. J. Marron, and M. A. Labrador. Real-time pedestrian tracking in indoor environments. *IEEE Latin-America Conference on Communications*, pages 1–6, 2014.

[41] E.A. Wan and R. Van Der Merwe. The Unscented Kalman Filter for nonlinear estimation. *Adaptive Systems for Signal Processing, Communications, and Control Symposium*, 2000.

[42] C. D. Wann, Y. J. Yeh, and C. S. Hsueh. Hybrid TDOA/AOA indoor positioning and tracking using Extended Kalman Filters. *IEEE 63rd Vehicular Technology Conference*, 92:1058 – 1062, 2006.

[43] R. Want, A. Hopper V. Falcao, and J. Gibbons. The active badge location system. *ACM Transactions on Information Systems*, 10:91–102, 1992.

[44] G. Welch and G. Bishop. An Introduction to the Kalman Filter. *Computer Graphics, Annual Conference on Computer Graphics & Interactive Techniques*, pages 1–41, 2001.

[45] S. Wielandt, A. V. Nieuwenhuyse, J. Goemaere, B. Nauwelaers, and L. D. Strycker. Evaluation of Angle of Arrival estimation for localization in multiple indoor environments. *Ubiquitous Positioning Indoor Navigation and Location Based Service*, pages 36–43, 2014.

[46] J. Wilson and N. Patwari. Radio tomographic imaging with wireless networks. *Proc. of IEEE Transactions on Mobile Computing*, 2010.

[47] J. Xiao, K. Wu, Y. Yi, L. Wang, and L. Ni. Pilot: Passive device-free indoor localization using channel state information. *IEEE 33rd International Conference on Distributed Computing Systems*, pages 236–245, 2013.

[48] J. Xiao, Z. Zhou, Y. Yi, and M. N. Lionel. A survey on wireless indoor localization from the device perspective. *ACM Computing Surveys*, 43:1–31, 2016.

[49] L. Xiaowei, M. Farah, and S. Hichem. Decentralized localization using radio-fingerprints and accelerometer in WSNs. *IEEE Transactions on Aerospace and Electronic Systems*, 51:242 – 257, 2015.

[50] Q. Xu, R. Zheng, W. Saad, and Z. Han. Device fingerprinting in wireless networks: Challenges and opportunities. *IEEE Communications Surveys and Tutorials*, 18:94 – 104, 2015.

[51] D. Yrn, M. Szilassy, B. Dil, and F. Gustafsson. A novel multi-step algorithm for low-energy positioning using GPS. *International Conference on Information Fusion*, pages 1469–1476, 2016.

[52] W. Zhang, X. Yang, L. Yu, and S. Liu. Sequential fusion estimation for RSS-based mobile robots localization with event-driven WSNs. *IEEE Transacations On Industrial Informatics*, 12:1519–1528, 2016.

[53] X. Zhang, J. Wang, Q. Gao, X. Ma, and H. Wang. Device-free wireless localization and activity recognition with deep learning. *IEEE International Conference on Pervasive Computing and Communication Workshops*, pages 1 – 5, 2016.